RSC Advances

ROYAL SOCIETY OF CHEMISTRY

www.rsc.org/advances

Effect of functionalized multi-walled carbon nanotubes on the microstructure and performances of PVDF membranes

Zongxue Yu [a,*] Guangyong Zeng [a] Yang Pan [a] Liang Lv [a] Hui Min [a] Lei Zhang [a] Yi He [b,*]

(a.College of Chemistry and Chemical Engineering, Southwest Petroleum University, Chengdu City, Sichuan Province 610500, People's Republic of China; b. State Key Laboratory of Oil & Gas Reservoir Geology and Exploitation, Southwest Petroleum University, Chengdu City, Sichuan Province 610500, People's Republic of China)

**Address correspondence to this author. Email: haiqingy@163.com, heyi@swpu.edu.cn, Phone and Fax: +86 02883037315*

Abstract: Functionalized multi-walled carbon nanotubes (f-MWCNTs) were synthesized by grafting carboxyl groups and 3-aminopropyltriethoxysilane (APTS) on the nanotube surface, respectively. A novel polyvinylidene fluoride (PVDF) membrane was prepared by incorporation of different dosages of APTS modification MWCNTs (A-MWCNTs) via the phase-inversion method. The dispersity of MWCNTs and compatibility between MWCNTs and polymer matrix were enhanced after functional modification. Field emission scanning electron microscope (FESEM) and atomic force microscopy (AFM) testing showed that A-MWCNTs/PVDF blend membranes exhibited superior surface morphology and pore structure. Because of a strong interfacial interaction with PVDF matrix, the mechanical strength of PVDF membranes was improved by adding A-MWCNTs and the optimum adding content was 2 wt%. More importantly, the bovine serum albumin (BSA) rejection of membranes increased significantly from 64.2% (nascent PVDF membranes) to 92.48% (A-MWCNTs/PVDF), which was attributed to the network structure of APTS. It can be expected that the blending modification of PVDF membranes by f-MWCNTs will have a bright and foreseeable application prospect.

Keywords: PVDF blend membranes; f-MWCNTs; Dispersion; Microstructure; Hydrophilicity

1. Introduction

In the field of hydrophilic modification of polyvinylidene fluoride (PVDF) membrane, incorporation of inorganic nanoparticles into membrane has been extensively studied because it is simple and can be produced at an industrial scale easily [1, 2]. Due to their superior properties such as strong activities, large surface areas and high mechanical strength, inorganic nanoparticles can not only increase membranes hydrophilicity and fouling resistance properties [3-6], but also improve the microstructure and mechanical strength of membranes [7]. These nanoparticles mainly include Al_2O_3 [8, 9], TiO_2 [10, 11], SiO_2 [12, 13], ZrO_2 [14] and Fe_3O_4 [15], etc. Carbon nanotubes (CNTs), with diameter ranging from one to dozens of nanometers, have received much attention both from theoretical and experimental studies since their discovery by Iijima in 1991 [16]. Recently, multi-walled carbon nanotubes (MWCNTs) have also attracted considerable interests in the field of membranes[17-19]. It has been reported that MWCNTs can help to accelerate mass transfer in the process of membrane pervaporation and make membrane exhibit better pore structure compared with pristine PVDF membrane [5, 20]. Besides, the pure water flux and the bovine serum albumin (BSA) rejection of PVDF/MWCNTs blend membranes had also increased markedly [21].

However, as we all know, the MWCNTs often take the form of aggregates, due to the huge specific surface areas, high aspect ratios and strong van der Waals forces [22]. To expand the

applications in the field of membranes, functionalized MWCNTs (f-MWCNTs) were used as additives in some reports [23]. Some hydrophilic functional groups such as carboxyl and amino, were generated on the surface of MWCNTs [24]. The results demonstrated that the diffusion rate between solvent and gels was accelerated by f-MWCNTs in the process of membrane preparation. The compatibility between f-MWCNTs and polymer matrix performed better and the permeability of f-MWCNTs/PVDF blend membranes have been further improved [25]. The nano-scale diameters and the large surface of the CNTs also helped to transform a membrane from ultrafiltration to nanofiltration [24]. In addition, some specific groups were used to decorate MWCNTs before blending with membranes, which can solve the practical problems during water-treatment process[26-29].

In this work, 3-aminopropyltriethoxysilane (APTS) was used to decorate MWCNTs (A-MWCNTs) to improve the dispersity of MWCNTs and compatibility between MWCNTs and polymer matrix, which can reduce the stress concentration points in blend membrane. A novel blend membrane A-MWCNTs/PVDF was prepared via the phase-inversion method, which has never been reported in literatures. For comparisons, MWCNTs/PVDF and carboxylated MWCNTs/PVDF (C-MWCNTs/PVDF) membranes were also studied. The results demonstrated that the interfacial interaction between MWCNTs and polymer matrix was enhanced, which was due to the long chain of APTS penetrating into PVDF matrix [30]. In addition, A-MWCNTs/PVDF exhibited better than MWCNTs/PVDF and C-MWCNTs/PVDF in the performances of microstructure, BSA rejection and mechanical strength.

2. Experimental

2.1. Materials

The PVDF (FR904) was supplied by Shanghai 3F New Materials Co. Ltd., China. Polyvinyl pyrrolidone (PVP), *N, N'*-dimethylacetamide (DMAc, ≥99.5%), and 3-aminopropyltriethoxysilane (APTS, ≥99%, 0.945 g/mL) were purchased from Chengdu Kelong Chemical Reagent Factory, China. Multi-walled carbon nanotubes (MWCNTs, diameter: 20-30 nm, length: 10-30 μm, purity >95%) were purchased from Chengdu organic chemicals Co. Ltd. Chinese Academy of Science. BSA (M_W=67,000) was purchased from Shanghai Ruji Bio Co. Ltd., China. All reagents were used without further purification.

2.2. Preparation of C-MWCNTs and A-MWCNTs

First of all, MWCNTs were modified by mixed acid (H_2SO_4:HNO_3=3:1) to obtain C-MWCNTs. Then, the C-MWCNTs were firstly treated with $SOCl_2$ to introduce the acyl groups. The samples were sonicated for 30 min with some ethanol and DI water in 250 ml breaker. The solutions were transferred into a three-necked flask and mixed with 10 ml of APTS. The system was refluxed at 80℃ for 1 h [31]. Finally, the A-MWCNTs were obtained after filtrating and drying in a vacuum oven. The modification of the C-MWCNTs with APTS is illustrated in Fig.1 [32].

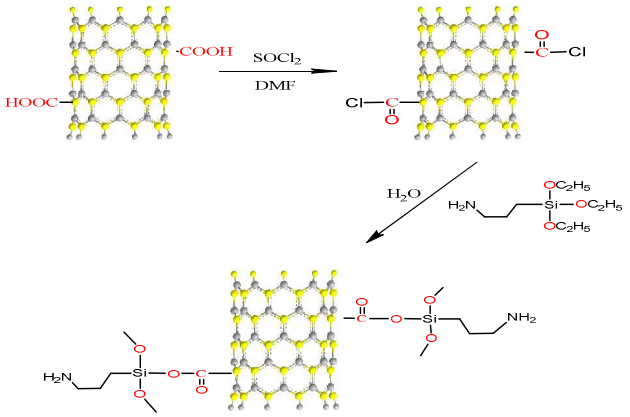

Fig.1. Illustration of the reaction between C-MWCNTs and APTS.

2.3. Preparation of membranes

All the membranes were synthesized by phase-inversion method, by using PVDF and PVP as solute material, DMAc as solvent, MWCNTs, C-MWCNTs and A-MWCNTs as additives, and DI water as non-solvent coagulation bath. C-MWCNTs and A-MWCNTs (0, 0.5, 1, 2 and 4 wt%)(based on PVDF weight) were added into DMAc solvent (80 g), and dispersed by ultrasonic cleaner for 30 min before addition of PVP (2 g) and PVDF (18 g) powders. Casting solution was stirred for 12 h at 343.15 K and then moved into a vacuum-drying oven over 12 h to release bubbles.

A casting knife was used to control the thickness of membranes (200 μm). To make sure that air bubbles were blocked and cannot be infiltrated in the casting solution, this process must be slow. The glass, coated with casting solution, was then immersed into DI water for 30 min. The membranes peeled off from glass plates were washed and soaked in DI water before ultrafiltration tests. To identify these membranes easily, they were denoted as MWCNTs/PVDF, C-MWCNTs/PVDF and A-MWCNTs/PVDF, respectively.

2.4 Characterization of ~~MWCNTs and~~ f-MWCNTs

The Fourier-transform infrared (FT-IR) (Beijing Beifen-Ruili Analytical Instrument, WQF-520) spectra were used to record the characteristic peaks of the C-MWCNTs and A-MWCNTs. To characterize the thermal stability of C-MWCNTs and A-MWCNTs, thermo-gravimetric analyzer (TGA) (Netzsch, STA449F3) was used. It was carried out at a heating rate of 10℃/min and in nitrogen atmosphere. The surface morphologies of C-MWCNTs and A-MWCNTs were examined by transmission electron microscopy (TEM) (JEOL, JEM-100CX) and the samples were sonicated and dispersed in ethanol solution.

2.5 Characterization of membranes

2.5.1 Morphologies

The morphologies of ~~MWCNTs/PVDF, C-MWCNTs/PVDF and A-MWCNTs/PVDF~~ membranes were probed by a field emission scanning electron microscope (FESEM)(ZEISS, ΣIGMA) with electron beam energies of 5 kV. To get cross-sections, the membranes were glaciated and fractured in liquid nitrogen. After being coated with gold, all samples were tested. Under different magnifications, the morphologies of ~~all blend~~ membranes were observed.

The surface morphologies of membranes were tested by atomic force microscopy (AFM)

(NSK, SPA300HV). It was manipulated in tapping-mode and the scan area was 10 μm×10 μm. The surface roughness parameters were reflected in relation to R_a, R_q, and R_z.

2.5.2 Permeation performances

The pure water flux and BSA rejection of all membranes were measured and evaluated by ultrafiltration experimental device (SINAP, SCM-300). Under the pressure of 0.1 MPa, all experiments were conducted and the newly prepared membranes should be pre-pressured for 0.5 h. The pure water flux (J) was defined as follows:

$$J = V/At \quad (1)$$

where t stands for the running time (h). V and A are the volume of water (L) and the effective area (m^2) of the membrane, respectively.

A newly prepared 1000 ppm BSA aqueous solution was used to carry out the tests of rejection. UV-spectrophotometer (SHIMADZU, UV-1800) was used to calculate the concentrations of BSA at 280 nm. The rejection of BSA (R) was defined by following equation:

$$R(\%) = \left(1 - \frac{C_p}{C_f}\right) \times 100 \quad (2)$$

where C_f is the initial BSA concentration (mg/L) and C_p is the final BSA concentration after permeation (mg/L).

2.5.3 The porosity and mean pore radius

The porosity ($\mathcal{E}$) of membranes was determined by the gravimetric method [33]. The membranes in DI water were removed and weighed after mopping. Then the wet membranes were dried to measure the dry weight. The following equation was used to calculate the porosity of membranes:

$$\varepsilon = \frac{(\omega_1 - \omega_2)/\rho_w}{(\omega_1 - \omega_2)/\rho_w + \omega_2/\rho_P} \quad (3)$$

where ω_1 and ω_2 are the weight of membranes in the wet and dry conditions (g), respectively. ρ_w and ρ_p are the water density (0.998 g/cm^3) and PVDF density (1.765 g/cm^3), respectively.

Guerout-Elford-Ferry equation was applied to calculate the mean pore radius (r_m) of the membrane [34]:

$$r_m = \sqrt{\frac{(2.9 - 1.75\varepsilon) \times 8\mu l J}{\varepsilon \times TMP}} \quad (4)$$

where μ and l are the water viscosity (8.9×10^{-4} Pa·s) and the membrane thickness (m), TMP stands for the operation pressure (0.1 MPa), respectively.

2.5.4 Mean contact angle measurement

The contact angle (CA) was measured with an instrument (Beijing Hake, XED-SPJ). At room temperature, 2.0 μl DI water was dropped on the surface of flat homogeneous membrane and CA was tested with water spreading over the membrane surface. Until there was no change in CA, the value was obtained. To minimize the experimental error, the CA of each membrane sample was measured three times at three different points.

2.5.5. Mechanical strength measurement

The mechanical strength of each membrane was evaluated by universal testing machine (Jinan Instrument, WDW-1000). Each prepared sample was 3.5 cm in length, 2.5 cm in width and 200 μm in thickness. The sample was measured at a stretching rate of 2 mm/min and each membrane was also tested three times at three different points.

3. Results and discussion

3.1. Characterization of MWCNTs and f-MWCNTs

3.1.1. FTIR analysis of MWCNTs and f-MWCNTs

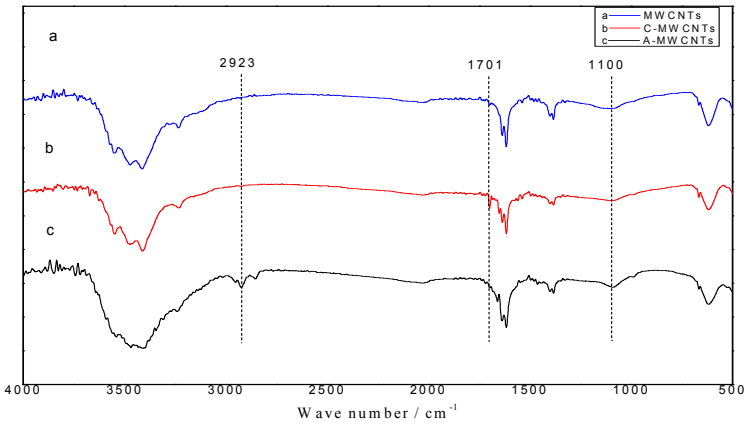

Fig.2. FTIR spectra of MWCNTs (a), C-MWCNTs (b) and A-MWCNTs(c).

The FTIR spectra of MWCNTs, C-MWCNTs and A-MWCNTs were shown in Fig.2. In comparison with raw MWCNTs, the FTIR spectra of C-MWCNTs and A-MWCNTs exhibited new peaks. The peaks appearing at 1620, 1701, and 3100-3600 cm^{-1} corresponded to -COOH and -OH functional groups onto the surface of C-MWCNTs [35]. Meanwhile, the new peaks of A-MWCNTs were referred to as $-CH_3$ (2856 cm^{-1}), $-CH_2$ (2923 cm^{-1}), and Si-O (1100 cm^{-1}) bonds [36], which confirmed that APTS was introduced into MWCNTs successfully. Generally, these hydrophilicity functional groups could not only improve the dispersion of C-MWCNTs and A-MWCNTs in aqueous solution, but also enhance the permeability and hydrophilicity of PVDF membranes. Then, these functionalized MWCNTs would be used for further blending with PVDF.

3.1.2. TGA of MWCNTs and f-MWCNTs

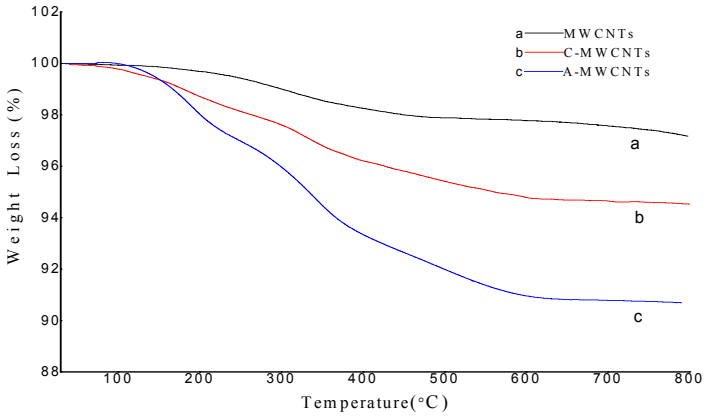

Fig.3. TGA curves of MWCNTs (a), C-MWCNTs (b) and A-MWCNTs (c).

The TGA curves of MWCNTs, C-MWCNTs and A-MWCNTs were presented in Fig.3. The weight loss ratio of MWCNTs was just 3.0%. However, there were two much higher weight losses of 5% and 10% between 300℃ and 600℃, which were referred to C-MWCNTs and A-MWCNTs. These weight losses were ascribed to the decomposition of carboxyl functional groups and organosilane functional groups respectively, which could further verify that the functionalization of MWCNTs had been achieved. These results were consistent with FTIR spectra and also similar to other experimental results [26] .

3.1.3 Dispersion images of MWCNTs and f-MWCNTs in DMAc

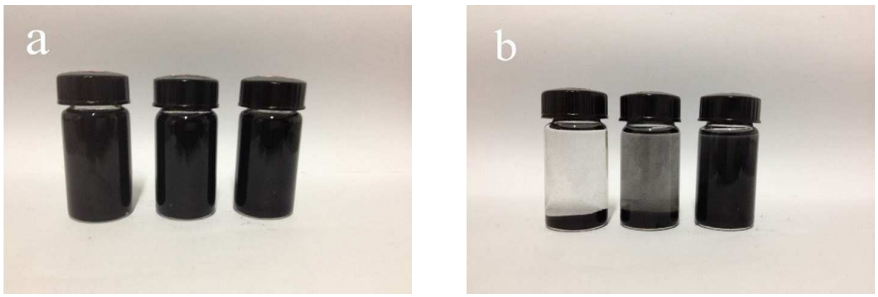

Fig.4.The dispersion images of MWCNTs (left), C-MWCNTs (medium) and A-MWCNTs (right) in DMAc (a and b are standing for 1h and 36 h after sonication, respectively).

Fig.4 showed the dispersion images of MWCNTs, C-MWCNTs and A-MWCNTs in DMAc. After sonication, both MWCNTs and f-MWCNTs were dispersed well. However, MWCNTs and DMAc segregated clearly after standing for 36 h. C-MWCNTs could still keep compatible to some extent in DMAc, which attributed to the introduction of hydroxyl and carboxyl groups [37]. It was interesting that the dispersion ~~result~~ of A-MWCNTs in DMAc was the best and excellent, which would utilize the properties of MWCNTs to the uttermost.

3.1.4 TEM observations of MWCNTs and f-MWCNTs

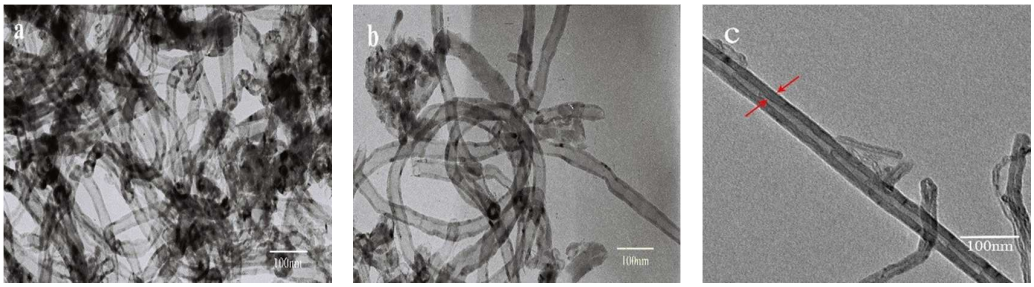

Fig.5. TEM images of MWCNTs (a), C-MWCNTs (b) and A-MWCNTs(c).

Fig.5 presented TEM images of MWCNTs (a), C-MWCNTs (b) and A-MWCNTs(c), which were dispersed in ethanol solution. We found that MWCNTs were held together and dispersed worse when compared with C-MWCNTs and A-MWCNTs. This phenomenon was related to MWCNTs intrinsic van der Waals forces [38]. Carboxyl acid treatment fractured the surface and shortened the length of MWCNTs at some places [35] in Fig.5b. With modification of APTS, the diameters of MWCNTs increased remarkably in Fig.5c. It demonstrated that APTS was introduced on the surface of MWCNTs successfully. Moreover, the dispersion of MWCNTs was improved after carboxyl and APTS treatment. Meanwhile, their surface seemed cleaner than before [24]. The red arrow in Fig.5c could prove that the wall of MWCNTs became thicker, which were decorated by APTS.

3.2. Morphology and microstructure of membranes

3.2.1 FESEM images

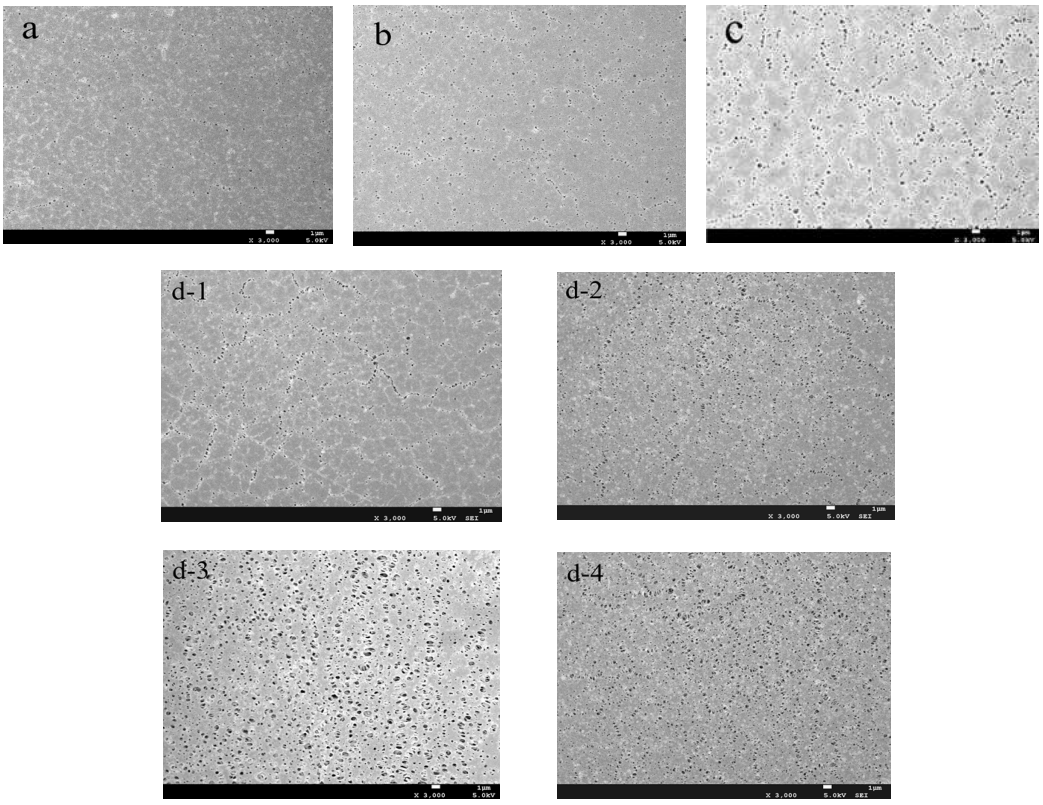

Fig.6. FESEM images of the top surfaces of different membranes

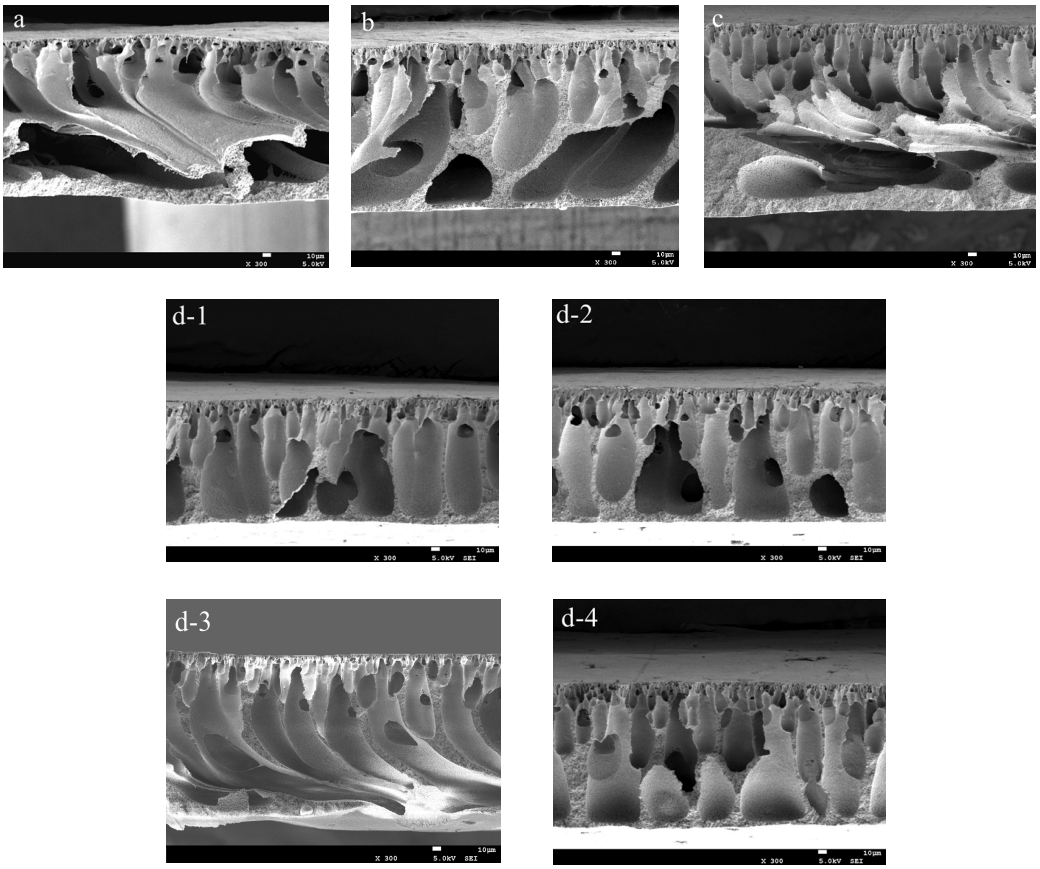

Fig.7.The cross-section morphologies of different membranes

The FESEM images of the top surfaces of nascent PVDF (a), 2wt% MWCNTs/PVDF (b), 2wt% C-MWCNTs/PVDF (c) and different dosages of A-MWCNTs/PVDF (d1~d4 for 0.5~4wt %) membranes were taken under 3000× magnification in Fig.6. The obvious variation of membrane's pore structures were observed from images. MWCNTs materials played an integral role in the process of membrane-formation because some surface characteristics, such as surface charge, could change the membrane microstructure. The mean pore sizes were increased with the addition of f-MWCNTs, which could be explained by the mechanism of phase separation. During the phase inversion, the rich oxygen-containing functional groups made f-MWCNTs become typical hydrophilic materials and accelerated the mass transformation between the solvent and non-solvent [20].

Accordingly, the cross-section morphologies of these membranes were shown in Fig.7, which were taken under 300× magnification. As could be seen from the figure, all the membranes belonged to an asymmetric porous structure, which had a thin upper skin layer and a finger-like porous sub-layer [39]. The cross-section of blend membranes becomes a little denser and the finger-like pores were wider than pure PVDF membrane. In the process of membrane preparation, the diffusion rate between solvent (DMAc) and gels (water) was accelerated by MWCNTs. Therefore, because of rapid mass transformation, larger pore channels were formed. In addition, A-MWCNTs/PVDF exhibited better microstructure than other membranes and it reached the best with 2wt% content of A-MWCNTs (d-3). It was clear that the additives enhanced thermodynamic

instability of the solution, which was propitious to phase separation. Also, the long chains of APTS were expected to penetrate into the matrix, which further enhanced thermodynamic instability of blend-casting solution, and it was inherently prone to phase separation. Thus, a quicker liquid–liquid phase separation and a less stable system appeared and formed a more porous structure of cross-section.

In general, the FESEM images indicated that the addition of MWCNTs and f-MWCNTs greatly influenced and improved the membrane structures, thereby altering the porosity and pore diameter of surface and inner microstructure.

3.2.3 AFM observations

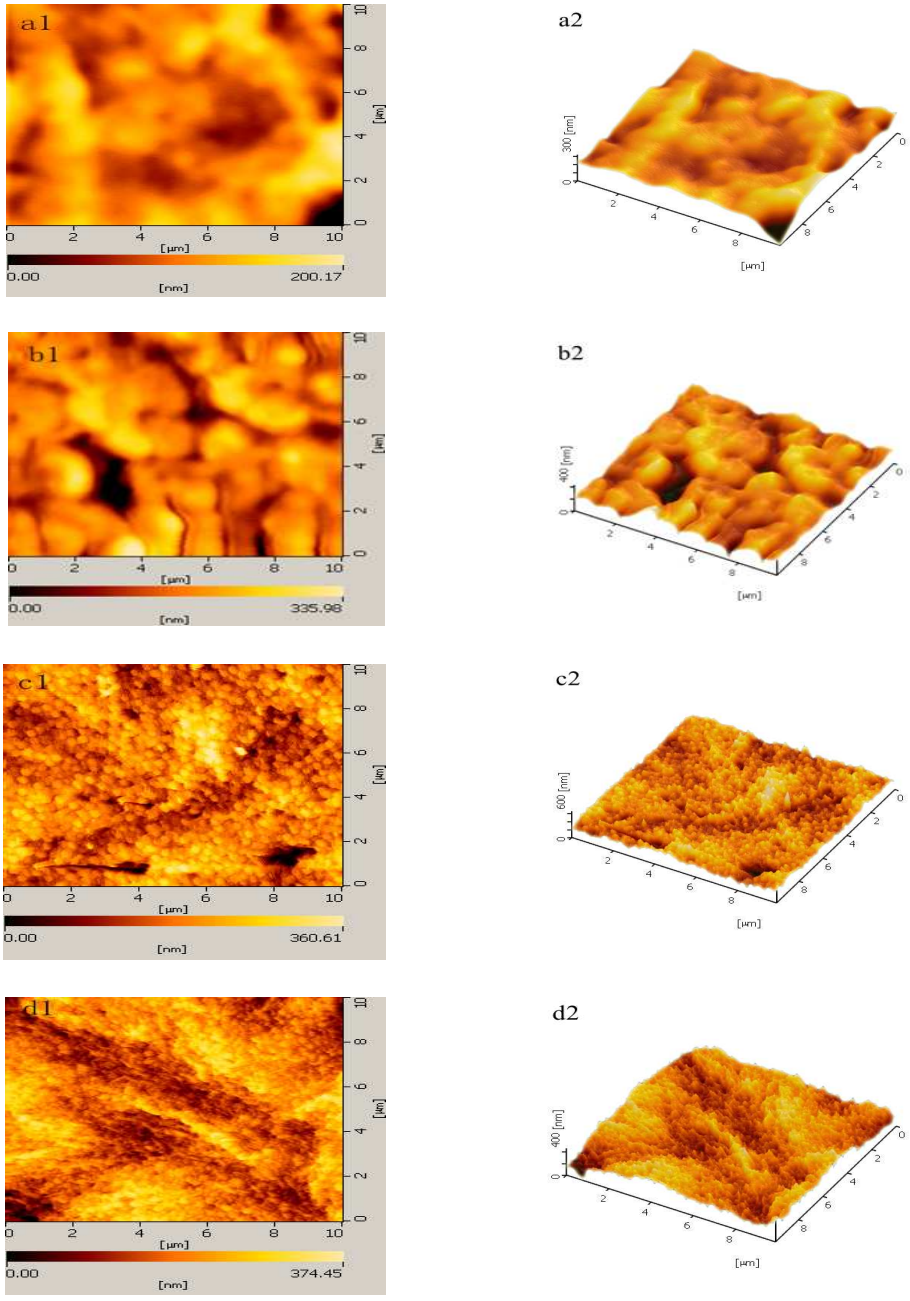

Fig.8. 2D (left) and 3D (right) AFM topography of (a) PVDF membrane, (b) 2wt%-MWCNTs/PVDF membrane, (c) 2wt%-C-MWCNTs/PVDF and (d) 2wt%-A-MWCNTs/PVDF.

Fig.8 showed the 2D and 3D AFM images of different types of membranes at a scan area of 10 μm×10 μm. Table 1 showed the roughness and surface area parameters obtained from analyzing the AFM images. The surface roughness of blend membranes were obviously higher than that of pristine PVDF membranes, and A-MWCNTs/PVDF membranes exhibited the largest R_a, R_q, and R_z (47.8nm, 58.6nm and 295.0nm). High surface area and roughness could increase the efficient filtration area, which led to the enhancement of pure water flux ultimately. Totally, MWCNTs could improve the microstructure and influence the hydrophilicity of PVDF membranes.

Table 1. Surface parameters of different PVDF blend membranes.

Membrane	Roughness			Surface area
	R_a (nm)	R_q (nm)	R_z (nm)	(μm^2)
PVDF	23.4	30.6	139.8	99.6
2% MWCNTs/PVDF	39.3	52.3	238.1	101
2% C-MWCNTs/PVDF	42.0	54.1	273.3	114.2
2% A-MWCNTs/PVDF	47.8	58.6	295.0	118

3.3 Pore and contact angle of membranes

Table 2. The detailed data of different kinds of membranes

Type of membrane	Porosity (%)	Mean Pore size (nm)	Contact angel (°)	Tensile strength (MPa)	Tensile strain (%)
PVDF	55.6	29.4	81.6±0.3	0.74±0.05	38.4±0.2
2% MWCNTs/PVDF	58.8	31.7	65.5±0.3	1.23±0.04	22.7±0.3
0.5% C-MWCNTs/PVDF	60.8	36.6	61.2±0.2	1.22±0.11	23.3±0.1
1% C-MWCNTs/PVDF	66.8	40.3	59.0±0.3	1.26±0.08	21.1±0.2
2% C-MWCNTs/PVDF	76.2	49.2	56.1±0.5	1.26±0.06	19.9±0.3
4% C-MWCNTs/PVDF	75.7	48.2	60.3±0.2	1.21±0.07	20.5±0.1
0.5% A-MWCNTs/PVDF	63.9	35.9	58.6±0.1	1.28±0.01	21.2±0.2
1% A-MWCNTs/PVDF	67.2	42.8	55.5±0.4	1.38±0.04	19.9±0.3
2% A-MWCNTs/PVDF	78.1	53.0	50.5±0.5	1.54±0.12	18.7±0.1
4% A-MWCNTs/PVDF	76.2	53.3	53.9±0.2	1.53±0.09	20.1±0.2

Table 2 showed the porosity, mean pore size and contact angle of different types of membranes. The porosity and mean pore sizes of PVDF membranes were increased significantly by adding f-MWCNTs, which were attributed to the contents of hydrophilic groups of f-MWCNTs and accelerated the exchange of solvent and non-solvent. However, they were reduced by adding more f-MWCNTs and the peak values of porosity and mean pore size were obtained with 2wt%

content of additives. Besides, some similar results were obtained in the test of CA. The CA of blend membranes were reduced and 2 wt% of additives gave the best result (56.1±0.5° for C-MWCNTs and 50.5±0.5° for A-MWCNTs), which were also attributed to the hydrophilic groups. Furthermore, the addition of MWCNTs could enhance the tensile strength and decrease the tensile strain of PVDF membranes, especially for A-MWCNTs. The APTS entangled with PVDF matrix and strengthened the interfacial interaction between PVDF and additives. Overall, the properties of membranes behaved optimum when the dosages of additives were 2 wt%. High amount of additives agglomerated together and could not produce their advantages to the utmost.

3.4 Permeation property of membranes

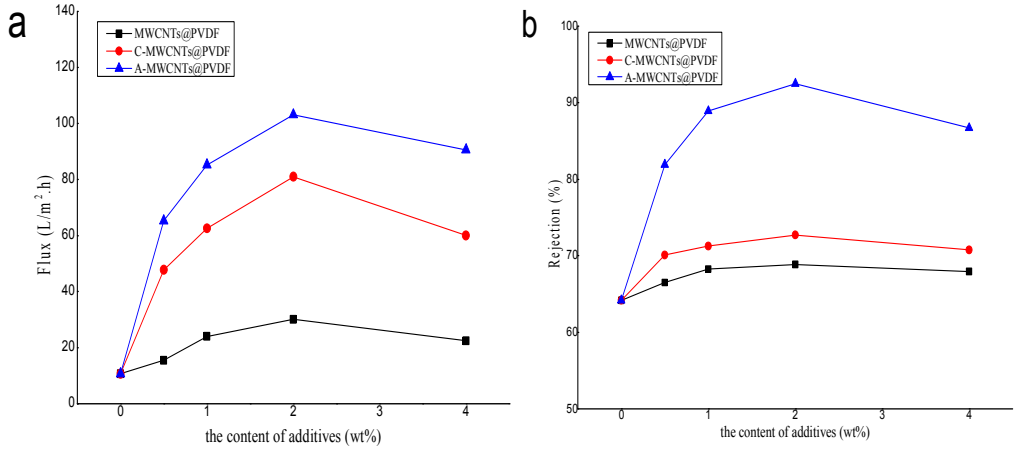

Fig.9. (a) pure water flux and (b) BSA rejection of various membranes.

The permeation properties of PVDF blend membranes were shown via Fig.9. The results indicated that MWCNTs, C-MWCNTs and A-MWCNTs were expected to increase the water permeation flux in Fig. 9(a), which could be explained as follows. Firstly, these additives had increased the surface area and roughness, which further increased the efficient filtration area and led to the enhancement of pure water flux[30]. Then, they had also improved porosity and pore size, which can promote more water to permeate the membrane per unit time[40]. When the dosage of these additives was 2 wt%, the water flux of various membranes reached a maximum. Besides, it ranked in the following order: MWCNTs/PVDF< C-MWCNTs/PVDF< A-MWCNTs/PVDF, which was due to the content of hydrophilic groups. It was clear that, the water flux of A-MWCNTs/PVDF membranes reached a maximum value of 103.16 L/ (m^2 .h) and increased nearly 870% when compared with pure PVDF membrane. In Fig. 9(b), the BAS rejection values of various membranes were observed. A-MWCNTs could obviously improve the BAS rejection of PVDF membranes. Rejection value reached a peak value of 92.48% when the content of additive was also 2 wt%. The schematic of the A-MWCNTs/PVDF adsorbing BSA is illustrated in Fig.10. The silanol in APTS molecules formed a network structure, which adsorbed the BSA molecules easily. It was clear that best permeation property of membranes were obtained when the dosage of additives was 2 wt%. MWCNTs and A-MWCNTs would agglomerate and the dispersion property was decreased in membranes.

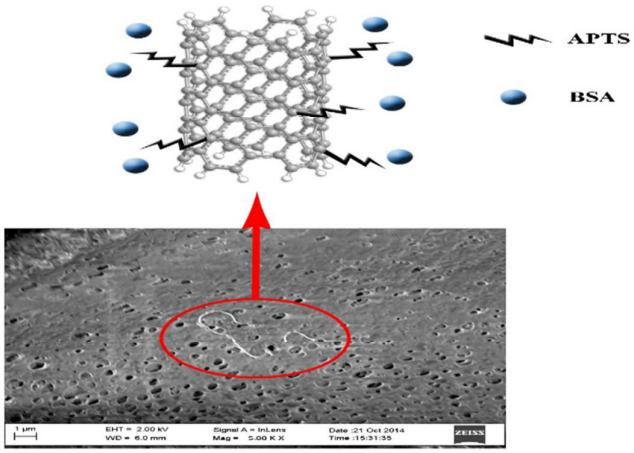

Fig.10.The schematic illustration of the A-MWCNTs/PVDF adsorbing BSA.

3.5 Mechanical strength of membranes

The mechanical strength of ultrafiltration membranes played a significant role in practical applications. The mechanical performances (including tensile strength and tensile strain) of different types of PVDF membranes were shown in Table 2. It was generally accepted that adding a small quantity of MWCNTs and f-MWCNTs, which had high aspect ratio, could increase the tensile strength. But excessive additives provided stress concentration points in the membrane, which caused the aggregation of MWCNTs in polymeric matrix. We found that the optimum content of the additive was 2 wt%. Besides, when compared with other membranes, the tensile strength of A-MWCNTs/PVDF blend membranes behaved better. The modification by APTS prevented stacking and aggregation of MWCNTs and thus improved the dispersion of MWCNTs in PVDF matrix. Furthermore, the APTS were supposed to penetrate into and entangle with PVDF matrix due to its long chains [41] and the interfacial interaction between PVDF and additives became stronger. However, the tensile strain of blend membranes declined and the membranes were not flexible any more. It demonstrated that f-MWCNTs could improve the microstructure and mechanical strength of PVDF membranes more effectively.

4. Conclusions

Through synthesizing f-MWCNTs/PVDF blend membranes and investigating their microstructure and performance, the following results were obtained:

(1) TEM observations and dispersion images indicated that the dispersion of MWCNTs was improved after functionalization, especially for APTS-modified, which was attributed to the increasing of hydrophilicity functional groups such as –COOH, -OH and –CO–NH–. AFM and FESEM showed that f-MWCNTs/PVDF blend membranes exhibited better microstructure than MWCNTs/PVDF blend membranes and pure PVDF membranes.

(2) The amount of f-MWCNTs obviously affected the hydrophilicity of PVDF membranes and the most suitable dosage was 2 wt%. The CA of membranes evidently decreased from 81.6° (pure PVDF) to 65.5° (MWCNTs/PVDF), 56.1° (C-MWCNTs/PVDF) and 50.5° (A-MWCNTs/PVDF). Owing to a network structure in APTS molecules, the BSA rejection of A-MWCNTs/PVDF increased significantly from 64.2% to 92.48%. Besides, APTS was supposed to penetrate into and entangle with PVDF matrix due to its long

chains, which strengthened the interfacial interaction between PVDF and additives and enhanced the mechanical strength of PVDF membranes.

What can be expected is that f-MWCNTs create a new chance to improve the microstructure and performance of PVDF membranes and have a bright future for practical application. In further studies, we will continue to explore the antifouling capability when these blend membranes are used to treat oily wastewater, which is seldom reported in the literature[42].

Acknowledgments

This work was financially supported by The Applied Basic Research Project in Sichuan Province (2013JY0099).

References

1. F. Liu, N. A. Hashim, Y. Liu, M. R. M. Abed and K. Li, *Journal of Membrane Science*, 2011, **375**, 1-27.
2. M. G. Buonomenna, *RSC Advances*, 2013, **3**, 5694-5740.
3. X. Li, R. Pang, J. Li, X. Sun, J. Shen, W. Han and L. Wang, *Desalination*, 2013, **324**, 48-56.
4. R. A. Damodar, S. J. You and H. H. Chou, *Journal of hazardous materials*, 2009, **172**, 1321-1328.
5. Y. Zhao, Z. Xu, M. Shan, C. Min, B. Zhou, Y. Li, B. Li, L. Liu and X. Qian, *Separation and Purification Technology*, 2013, **103**, 78-83.
6. Q. Zhao, J. Qian, M. Zhu and Q. An, *Journal of Materials Chemistry*, 2009, **19**, 8732-8740.
7. R. Bai, H. Wang, P. Zhang, B. Xiao, B. Jiang and G. Zhou, *RSC Advances*, 2015, **5**, 57147-57154.
8. X. S. Yi, S. L. Yu, W. X. Shi, N. Sun, L. M. Jin, S. Wang, B. Zhang, C. Ma and L. P. Sun, *Desalination*, 2011, **281**, 179-184.
9. L. Yan, S. Hong, M. L. Li and Y. S. Li, *Separation and Purification Technology*, 2009, **66**, 347-352.
10. S. S. Madaeni, S. Zinadini and V. Vatanpour, *Journal of Membrane Science*, 2011, **380**, 155-162.
11. X. Cao, J. Ma, X. Shi and Z. Ren, *Applied Surface Science*, 2006, **253**, 2003-2010.
12. Y. Zhan, R. Zhao, Y. Lei, F. Meng, J. Zhong and X. Liu, *Applied Surface Science*, 2011, **257**, 4524-4528.
13. X. Zuo, W. Shi, Z. Tian, S. Yu, S. Wang and J. He, *Desalination*, 2013, **311**, 150-155.
14. G. C. A. Bottino*, A. Comite, *Desalination* 2002, **14**, 35-40.
15. Z.-Q. Huang, F. Zheng, Z. Zhang, H.-T. Xu and K.-M. Zhou, *Desalination*, 2012, **292**, 64-72.
16. S. Iijima, *Nature*, 1991, **354**, 56-58.
17. T. L. S. Silva, S. Morales-Torres, J. L. Figueiredo and A. M. T. Silva, *Desalination*, 2015, **357**, 233-245.
18. J. Nunes-Pereira, C. M. Costa, R. Leones, M. M. Silva and S. Lanceros-Méndez, *Solid State Ionics*, 2013, **249–250**, 63-71.
19. B. Wu, X. Li, D. An, S. Zhao and Y. Wang, *Journal of Membrane Science*, 2014, **462**, 62-68.
20. I. M. Wienk, R. M. Boom, M. A. M. Beerlage, A. M. W. Bulte, C. A. Smolders and H.

Strathmann, *Journal of Membrane Science*, 1996, **113**, 361-371.
21. J. Zhang, Z. Xu, W. Mai, C. Min, B. Zhou, M. Shan, Y. Li, C. Yang, Z. Wang and X. Qian, *Journal of Materials Chemistry A*, 2013, **1**, 3101-3111.
22. S. Chatterjee, F. Nafezarefi, N. H. Tai, L. Schlagenhauf, F. A. Nüesch and B. T. T. Chu, *Carbon*, 2012, **50**, 5380-5386.
23. M. Irfan, A. Idris, N. M. Yusof, N. F. M. Khairuddin and H. Akhmal, *Journal of Membrane Science*, 2014, **467**, 73-84.
24. P. Shah and C. N. Murthy, *Journal of Membrane Science*, 2013, **437**, 90-98.
25. H.-P. Xu, W.-Z. Lang, X. Yan, X. Zhang and Y.-J. Guo, *Journal of Membrane Science*, 2014, **467**, 142-152.
26. X.-Q. Liu, S.-Q. Shen, R. Wen, W. Yang, B.-H. Xie and M.-B. Yang, *Composites Part B: Engineering*, 2013, **53**, 9-16.
27. K. H. Chan, E. T. Wong, M. I. Khan, A. Idris and N. M. Yusof, *Journal of Industrial and Engineering Chemistry*, 2014, **20**, 3744-3753.
28. S. S. Madaeni, S. Zinadini and V. Vatanpour, *Separation and Purification Technology*, 2013, **111**, 98-107.
29. S. S. Madaeni, S. Zinadini and V. Vatanpour, *Separation and Purification Technology*, 2011, **80**, 155-162.
30. Z. Xu, J. Zhang, M. Shan, Y. Li, B. Li, J. Niu, B. Zhou and X. Qian, *Journal of Membrane Science*, 2014, **458**, 1-13.
31. e. a. Hye Jin Park., *Langmuir*, 2008, **24**, 10467-10473.
32. N. Ardès-Guisot, J.-O. Durand, M. Granier, A. Perzyna, Y. Coffinier, B. Grandidier, X. Wallart and D. Stievenard, *Langmuir*, 2005, **21**, 9406-9408.
33. Z. Cui, N. T. Hassankiadeh, S. Y. Lee, J. M. Lee, K. T. Woo, A. Sanguineti, V. Arcella, Y. M. Lee and E. Drioli, *Journal of Membrane Science*, 2013, **444**, 223-236.
34. V. Vatanpour, S. S. Madaeni, R. Moradian, S. Zinadini and B. Astinchap, *Separation and Purification Technology*, 2012, **90**, 69-82.
35. J. Ma, Y. Zhao, Z. Xu, C. Min, B. Zhou, Y. Li, B. Li and J. Niu, *Desalination*, 2013, **320**, 1-9.
36. S. J. J. Titinchi and H. S. Abbo, *Catalysis Today*, 2013, **204**, 114-124.
37. Y. He, Z. Xu, Q. Yang, F. Wu and L. Liang, *Journal of Nanoparticle Research*, 2015, **17**.
38. E. Celik, L. Liu and H. Choi, *Water Research*, 2011, **45**, 5287-5294.
39. A. Bottino, G. Camera-Roda, G. Capannelli and S. Munari, *Journal of Membrane Science*, 1991, **57**, 1-20.
40. V. Vatanpour, S. S. Madaeni, A. R. Khataee, E. Salehi, S. Zinadini and H. A. Monfared, *Desalination*, 2012, **292**, 19-29.
41. Z. Xu, J. Zhang, M. Shan, Y. Li, B. Li, J. Niu, B. Zhou and X. Qian, *Journal of Membrane Science*, 2014, **458**, 1-13.
42. M. Padaki, R. Surya Murali, M. S. Abdullah, N. Misdan, A. Moslehyani, M. A. Kassim, N. Hilal and A. F. Ismail, *Desalination*, 2015, **357**, 197-207.